Astron. Astrophys. 356, 975–988 (2000)

ASTRONOMY AND ASTROPHYSICS

Internal shock model for microquasars

C.R. Kaiser, R. Sunyaev, and H.C. Spruit

Max-Planck-Institut für Astrophysik, Karl-Schwarzschild-Strasse 1, 85740 Garching, Germany

Received 22 December 1999 / Accepted 3 February 2000

Abstract. We present a model for the radio outbursts of microquasars based on the assumption of quasi-continuous jet ejection. The jets are 'lit up' by shock fronts traveling along the jets during outbursts. The shocks accelerate relativistic particles which emit the observed synchrotron radiation. The observed comparatively flat decay light curves combined with gradually steepening spectral slopes are explained by a superposition of the radiation of the aging relativistic particle population left behind by the shocks. This scenario is the low energy, time-resolved equivalent to the internal shock model for GRBs. We show that this model predicts energy contents of the radiating plasma similar to the plasmon model. At the same time, the jet model relaxes the severe requirements on the central source in terms of the rate at which this energy must be supplied to the jet. Observations of 'mini-bursts' with flat spectral slopes and of infrared emission far from the source centre suggest two different states of jet ejections: (i) A 'mini-burst' mode with relatively stable jet production and weak radio emission with flat spectra and (ii) an outburst mode with strong variations in the jet bulk velocities coupled with strong radio emission with steeper spectra. We also show that the continuous jets in microquasars should terminate in strong shocks and possibly inflate radio lobes similar to extragalactic jet sources. We investigate the possibility of testing the predictions of this model with resolved radio observations. Finally, we suggest that Doppler-shifted X-ray iron lines, and possibly H-α lines, may be emitted by the jet flow of microquasars if thermal instabilities analogous to those in SS433 exist in their jets.

Key words: shock waves – stars: binaries: general – stars: individual: GRS 1915+105 – radio continuum: stars

1. Introduction

The number of stellar mass black hole candidates known to produce jets has increased considerably over recent years. While SS433 was for a long time thought to be a rather exotic object, advances in X-ray astronomy have dramatically increased the number of known galactic X-ray binaries (van Paradijs 1995). At least nine of these sources subsequently showed evidence for the production of relativistically moving jets. Mirabel & Rodríguez (1999) give an excellent review on the observational and theoretical status of these objects, the microquasars.

The presence of relativistically moving material in these sources was discovered during radio observations. During times of strongly enhanced radio emission, which in the following we will refer to as radio outbursts, the emission region can often be resolved into at least two components. These components are observed to separate in opposite directions over a fews tens of days (i.e. Mirabel & Rodríguez 1994). The projected velocity of the component traveling on a trajectory towards the observer can exceed the speed of light, if its intrinsic velocity is large (e.g. Rybicki & Lightman 1979). In addition to the apparently superluminal nature of the jet components, their propagation has been observed to slow down only in one case (XTE J1748-288, Hjellming et al. 1999). This constant expansion speed led to the interpretation of practically ballistic trajectories of discrete plasmon ejections as explanation for the observed radio components (e.g. Mirabel & Rodríguez 1999).

Although suggested for the jets of SS433 (Hjellming & Johnston 1988), models with quasi-permanent jet production have received little attention in the case of microquasars. This is somewhat surprising given the large number of similarities they show with jet producing extragalactic sources like quasars (hence the name microquasars) and radio galaxies (e.g. Mirabel & Rodríguez 1998). In these cases there is little doubt that apart from some possible minor intermittency of the jet production mechanism for some sources (i.e. Reynolds & Begelman 1997) the jet flow is practically continuous.

In this paper we endeavour to close this gap by the development of a continuous jet model for microquasars to explain the radio outbursts observed in these sources. The model is based on the idea of internal shocks in jets (Rees 1978) which was successfully applied to Gamma Ray Bursts (GRB) (Rees & Meszaros 1994). In Sect. 2 we briefly review the plasmon model and discuss possible improvements on this within the jet picture. We develop the treatment of the relativistic jet flow in Sect. 3 and discuss the evolution of the synchrotron emission resulting from the internal shock in Sect. 4. The model is then applied to the probably best studied radio outburst of any microquasar, the March 1994 event in GRS 1915+105 (Mirabel & Rodríguez 1994) in Sect. 5. The properties of the jet of GRS 1915+105

Send offprint requests to: ckaiser@mpa-garching.mpg.de

like its energy content are derived from the model in Sect. 6. In Sect. 7 we consider the implications of a continuous jet for the interaction of microquasars with their environment. Finally, in Sect. 8 we summarise some observational consequences of our model which may be used to test the model with future observations.

2. Plasmons or jets?

Atoyan & Aharonian (1999) developed a model which is intended to reconcile the idea of discrete magnetised plasmon ejections during radio outbursts with the observed lightcurve and spectral behaviour in the radio waveband. They find that a single population of relativistic particles accelerated at the time of the ejection of the plasmons cannot explain the observations. The energy losses of the relativistic particles due to synchrotron radiation would lead to a sharp cut-off in the radio spectrum moving to lower frequencies as the plasmons expand and travel outwards. This is quite different from the observed rather gentle steepening of the spectrum. Atoyan & Aharonian (1999) also show that a continuous replenishment of relativistic particles to the plasmons alone cannot solve this problem because in this case the spectral cut-off moves to higher frequencies with time. They therefore postulate that the relativistic particles in the plasmons during the March 1994 event in GRS 1915+105 were continuously replenished, presumably by a shock at the side of the plasmons pointing towards the source centre, but also suffered energy dependent escape losses.

To fit the observations the scenario proposed by Atoyan & Aharonian (1999) requires that the mean free path of the most energetic relativistic particles in the magnetised plasmons is comparable to or exceeds the physical dimensions of the plasmons. This implies that these particles travel through the plasmons producing synchrotron emission but then leave them without scattering once off irregularities in the magnetic field or other particles. This is difficult to reconcile with the requirement that in order to be accelerated to relativistic velocities in the shock regions the mean free path in these regions must be short to ensure many shock crossings. If the accelerating shocks are close to the plasmons, this then means that the properties of the plasma change dramatically over short distances. Moreover, it is not clear in this scenario why the synchrotron emission is not completely dominated by the contribution of the shocks themselves.

In this paper we propose a different scenario to explain the observed properties of the radio emission of microquasars during outbursts. This is based on the assumption that microquasars may produce continuous jets for a long time before the actual outburst occurs and may well do so permanently (see also Levinson & Blandford 1996a, b). The outbursts in our model are then caused by two shocks traveling along these continuous jets which accelerate the required relativistic particles in situ. After the shock has passed a particular region in one of the jets, this region continues to contribute to the total emission until the cut-off in the specific spectrum of this region moves below the observing frequency. The jet components observed in microquasars are in general not resolved and so the measured flux is the integrated emission from all the jet regions passed by the shock which are still emitting at the relevant frequency. This implies that the observed spectrum is steeper than that of the jet region immediately behind the shock where radiation losses are still negligible. The variation of the strength of the magnetic field and of the number of relativistic particles accelerated by the shock along the jet then give rise to a slowly steepening radio spectrum. This effect was discussed in the case of the radio hot spots of powerful extragalactic radio sources by Heavens & Meisenheimer (1987).

Our investigation is based on the jet model of Blandford & Rees (1974) and Marscher & Gear (1985). A similar approach to explain the synchrotron self-Compton emission of extragalactic jets was taken by Ghisellini et al. (1985). They develop a numerical scheme to follow the evolution of the energy spectrum of the relativistic particles downstream of the jet shock taking into account radiative as well as adiabatic energy losses. They also include synchrotron self-absorption in this calculation. Since we are mainly interested in the radio emission of the jets of microquasars on rather large scales ($\sim 10^{14}$m), we can neglect any Compton scattering and absorption effects on the energy spectrum. In this case only adiabatic and synchrotron losses are important and we can use the analytic solution for the evolution of the energy spectrum of the relativistic electrons derived by Kaiser et al. (1997).

The underlying physical processes of the model presented here are very similar to the internal shock model proposed as explanation for GRB (Rees & Meszaros 1994). The same scenario has also been invoked to explain the X-ray and γ-ray emission of extragalactic jets (Ghisellini 1999). In the internal shock model the energy of the shock traveling along the jet is thought to be supplied by the collision of fast shells of jet material with slower ones (Rees 1978). In the case of GRB this energy is released practically instantaneously leading to the extremely short duration of the observed bursts of emission. In extragalactic jets the shell collision may take longer but the large distance to these objects makes it difficult to separate the contributions of multiple collision to the total emission. As outlined above, we argue in this paper that the jets of microquasars provide us with the possibility to observe the development of internal shocks in jets resolved both in space and time.

3. Dynamics of the jet

We follow Marscher & Gear (1985) and Ghisellini et al. (1985) in the assumption that all relevant physical quantities of the jet and the jet material are simple power law functions of the unprojected distance from the source centre, R. The shock traveling along the jet will compress the jet material but we will assume that it does not change the behaviour of the physical quantities as a function of the distance from the source centre. The radius of the cross section of the jet is assumed to follow $r \propto R^{a_1}$. For a freely expanding, conical jet $a_1 = 1$. The energy density of the magnetic field as measured in the rest frame of the jet material is then given by $u'_{\rm B} = u'_{\rm B}(R_{\rm o})(R/R_{\rm o})^{a_2}$, where energy

flux conservation would require $a_2 = -2a_1$. Here and in the following dashes denote quantities measured in the rest frame of the jet material moving at relativistic speeds while quantities measured in the frame of the observer are undashed.

The two frames of reference, the rest frame of the observer and that of the shocked jet material, are defined such that the origins of both coincide when the radio outbursts starts, i.e. when the shocks are formed in the centre of the source and start traveling outwards. Consider a section of the jet after the shock has passed through it. At time t this section is located at

$$R_{\rm ob} = \sin\theta R = \sin\theta v_{\rm s} t/(1 \pm \beta_{\rm j}\cos\theta), \quad (1)$$

in the rest frame of the observer. Here, θ is the angle of the jet to the line of sight and R is the unprojected distance of the jet section from the centre of the source, i.e. the origin of the observer's rest frame. $v_{\rm s}$ is the deprojected velocity of the shock as measured in the rest frame of the observer and $\beta_{\rm j} = v_{\rm j}/c$ is the deprojected velocity of the shocked jet material in this frame in units of the speed of light. The expression in brackets in Eq. (1) takes account of the Doppler shifted time measurements taken in the observer's frame caused by the receding (+) or approaching (−) component of the motion of the jet material (e.g. Rybicki & Lightman 1979). Transforming t and R to the frame comoving with the jet material we find

$$t' = \gamma_{\rm j}\left(\frac{t}{1 \pm \beta_{\rm j}\cos\theta} - \frac{v_{\rm j}R}{c^2}\right) \quad (2)$$

$$R' = \gamma_{\rm j}\left(R - \frac{v_{\rm j}t}{1 \pm \beta_{\rm j}\cos\theta}\right), \quad (3)$$

where $\gamma_{\rm j}$ is the Lorentz factor corresponding to the velocity of the shocked jet material, $v_{\rm j}$. For the origin of the comoving rest frame, $R' = 0$, we recover from Eqs. (2) and (3) the well-known result $t' = t\delta_{\pm}$ with the usual relativistic Doppler factor $\delta_{\pm} = [\gamma_{\rm j}(1 \pm \beta_{\rm j}\cos\theta)]^{-1}$. Since the shock moves along the jet, most of the observed emission is not produced at the origin of the comoving frame but at $R' \neq 0$. Suppose the section of the jet introduced above was passed by the shock at time $t'_{\rm s}$ as measured in the frame comoving with the shocked gas. Since this section is at rest in this frame, it is subsequently located at $R'_{\rm s} = v'_{\rm s}t'_{\rm s}$, where $v'_{\rm s}$ is the velocity of the shock as measured in the shocked gas' frame. Using this and substituting R from Eq. (3) in Eq. (2) yields

$$t' = t\delta_{\pm} - \frac{v_{\rm j}v'_{\rm s}t'_{\rm s}}{c^2}. \quad (4)$$

This expression illustrates the fact that the emission we observe at a given time t from different parts of the jet was not produced simultaneously in the frame of the shocked gas.

We assume that only those parts of the jet contribute to the total emission which have been passed by the shock. The emission regions within the jet can therefore be labeled with their 'shock time', $t'_{\rm s}$, and are observed at the intrinsic time t' given by Eq. (4). Since $t' \geq t'_{\rm s} \geq 0$, this implies $t\delta_{\pm}c^2/(c^2 + v_{\rm j}v'_{\rm s}) \leq t' \leq t\delta_{\pm}$. For convenience we introduce the ratio $\tau(t') = R/R_{\rm o} = \gamma_{\rm j}(v'_{\rm s}t'_{\rm s} + v_{\rm j}t')/R_{\rm o}$, where we have used Eqs. (2) and (3).

4. Synchrotron emission of the jet

4.1. Energy losses of the relativistic electrons

We assume that the shock passing through the jet material accelerates a population of relativistic electrons and/or positrons. During the acceleration process and afterwards these relativistic particles are subject to energy losses due to the approximately adiabatic expansion of the jet material and synchrotron radiation. To determine the exact form of the energy spectrum of the relativistic particles in a given jet region the kinetic equation including acceleration and energy terms must be solved. Heavens & Meisenheimer (1987) present analytic and numerical solutions for some simplified cases. They find that the energy spectrum follows a power law with a high energy cut-off. The cut-off occurs at the energy for which energy gains due to shock acceleration balance the synchrotron energy losses (e.g. Drury 1983). The cut-off becomes steeper further downstream from the shock. For simplicity we assume that the relativistic particles in a given jet region are initially accelerated at a time $t'_{\rm s}$ during a short time interval $dt'_{\rm s}$ to a power law spectrum with a sharp high energy cut-off at $\gamma_{\rm max}(t'_{\rm s})$. In terms of the number of particles this can be expressed by

$$N'(\gamma_{\rm s})d\gamma_{\rm s} = \begin{cases} \dot{N}'_{\rm o}(t'_{\rm s})\gamma_{\rm s}^{-p}d\gamma_{\rm s}dt'_{\rm s} & ;\gamma_{\rm s} \leq \gamma_{\rm max} \\ 0 & ;\gamma_{\rm s} > \gamma_{\rm max}. \end{cases} \quad (5)$$

Here $\dot{N}'_{\rm o}(t'_{\rm s})$ is the rate at which relativistic particles are accelerated in the jet by the shock at time $t'_{\rm s}$. The normalisation of this energy spectrum and the position of the high energy cut-off depend on the local conditions for diffusion in the jet (e.g. Drury 1983). These are not straightforward to estimate and we therefore assume for simplicity that the initial high energy cut-off of the relativistic particles freshly accelerated at time $t'_{\rm s}$ is independent of $t'_{\rm s}$. In the internal shock model for GRB the shock is caused by the collision of shells of jet material moving at different velocities. For GRB it is implicitly assumed that the collision energy is dissipated very close to instantaneously. In the case of microquasars the propagation of the shock is resolved in time. For the normalisation of Eq. (5) we therefore assume

$$\dot{N}'_{\rm o}(t'_{\rm s}) = \dot{N}'_{\rm o}(R_{\rm o})e^{-R_{\rm s}/(R_{\rm o}a_4)}, \quad (6)$$

where $R_{\rm s}$ is the position of the shock at time $t'_{\rm s}$ and a_4 a model parameter. This implies that the rate at which the collisional energy is dissipated and partly conferred to the relativistic particles is almost constant for $R_{\rm s}/R_{\rm o} < a_4$ and decreases exponentially at larger distances. The onset of the exponential behaviour then signifies the point at which almost all of the collisional energy has been dissipated and the shock starts to weaken significantly. This would coincide with the time at which the two colliding shells have practically merged into one. Alternatively, in only intermittently active sources the exponential decrease may be caused by the shock, and therefore the fast shell causing the shock, reaching the end of the jet.

After the passage of the shock the relativistic particles continue to loose energy. The rate of change of the Lorentz factor

of these particles due to the nearly adiabatic expansion of the jet is given by (e.g. Longair 1981)

$$\frac{d\gamma}{dt'} = -\frac{\gamma}{3\Delta V'}\frac{d\Delta V'}{dt'}, \tag{7}$$

where $\Delta V'$ is the volume of the jet region the particles are located in. We assume that the bulk velocity of the shocked jet material is constant and this implies that the jet is only expanding perpendicular to the jet axis, i.e. $\Delta V' \propto (R/R_{\rm o})^{2a_1} = \tau^{2a_1}$. Changing variables from t' to τ' then yields

$$\frac{d\gamma}{d\tau'} = -\frac{2a_1}{3}\frac{\gamma}{\tau'}. \tag{8}$$

Energy losses due to synchrotron radiation give

$$\frac{d\gamma}{d\tau'} = -\frac{4}{3}\frac{\sigma_{\rm T}}{m_{\rm e}c^2}\gamma^2 u'_{\rm B}(R_{\rm o})\frac{R_{\rm o}}{\gamma_{\rm j}v_{\rm j}}\tau'^{-2a_1}, \tag{9}$$

where $\sigma_{\rm T}$ is the Thompson cross section and $m_{\rm e}$ the rest mass of an electron. By summing Eqs. (8) and (9) and integrating we find the Lorentz factor γ at time t' of those electrons which had a Lorentz factor $\gamma_{\rm s}$ at time $t'_{\rm s}$ (see also Kaiser et al. 1997)

$$\gamma(t',t'_{\rm s}) = \frac{\gamma_{\rm s}\tau'(t')^{-2/3a_1}}{\tau'(t'_{\rm s})^{-2/3a_1} + b_1(t',t'_{\rm s})\gamma_{\rm s}}, \tag{10}$$

with

$$b_1(t',t'_{\rm s}) = \frac{4}{3a_3}\frac{\sigma_{\rm T}}{m_{\rm e}c}\frac{u_{\rm B}(R_{\rm o})R_{\rm o}}{\gamma_{\rm j}v_{\rm j}}\left[\tau'(t')^{a_3} - \tau'(t'_{\rm s})^{a_3}\right] \tag{11}$$

and

$$a_3 = 1 - 2\left(a_2 + \frac{a_1}{3}\right). \tag{12}$$

The number of relativistic particles with a Lorentz factor in the range γ to $\gamma + d\gamma$ in the jet region overtaken by the jet shock at time $t'_{\rm s}$ is therefore given by

$$N'(\gamma)d\gamma = \begin{cases} \dot{N}'_{\rm o}(t'_{\rm s})\gamma^{-p}b_2 \\ \times\tau'(t')^{-2/3a_1}d\gamma dt'_{\rm s} & ;\gamma \le \gamma_{\rm max}(t') \\ 0 & ;\gamma > \gamma_{\rm max}(t'), \end{cases} \tag{13}$$

with

$$b_2 = \left[\tau'(t')^{-2/3a_1} - b_1(t',t'_{\rm s})\gamma\right]^{p-2}\tau'(t'_{\rm s})^{2/3a_1(p-1)}. \tag{14}$$

Note here that the high energy cut-off, $\gamma_{\rm max}(t')$, also evolves according to Eq. (10).

4.2. Synchrotron emission

The synchrotron emission of the relativistic particles at time t' in the region of the jet overtaken by the shock at time $t'_{\rm s}$ is given by

$$dP'_{\nu'} = \int_{\gamma_{\rm min}}^{\gamma_{\rm max}}\frac{4}{3}\sigma_{\rm T}cu_{\rm B}(t',t'_{\rm s})\gamma^2\Phi(\nu',\gamma)N'(\gamma)d\gamma, \tag{15}$$

where $\Phi(\nu',\gamma)$ is the synchrotron emission spectrum of a single electron with Lorentz factor γ. Here we assume that the magnetic field in the jet is tangled on scales smaller than the radius of the jet. This then implies that $\Phi(\nu',\gamma) = \bar{F}(\gamma)/\nu_{\rm c}$, where $\bar{F}$ is one of the synchrotron integrals normalised to give $\int_1^\infty \bar{F}(\gamma)d\gamma = 1$ (e.g. Shu 1991). To get the total emission of the jet behind the jet shock we have to sum the contributions of all the regions labeled with their shock times $t'_{\rm s}$ within the jet. From Eq. (13) we see that this implies integrating Eq. (15) over $t'_{\rm s}$. This integration must be performed numerically. Finally, to compare the model results with the observations we have to transform to the rest frame of the observer, $P_\nu = P'_{\nu'}\delta_\pm^3$. Note here that the luminosity inferred from the observations at frequency ν was emitted in the gas rest frame at a frequency $\nu' = \nu/\delta_\pm$.

As mentioned above, the steepening of the radio spectrum of the superluminal jet components observed during outbursts of microquasars is caused by the integrated emission from an extended region of the jet. The further away from the shock the emission is created in the jet, the lower the cut-off in the energy spectrum of the relativistic electrons will be. However, if the jet region contributing to the total emission is not too large the properties of the energy spectrum will not change dramatically within this region. In this case we may estimate the approximate location of the break in the radio spectrum beyond which the spectrum steepens significantly. Most of the energy lost by relativistic particles is radiated at their critical frequency, $\nu_{\rm c} = (3/2)\,\nu_{\rm L}\gamma^2$, where $\nu_{\rm L}$ is the Larmor frequency. Defining the break frequency, $\nu_{\rm b}$, as the critical frequency of the most energetic particles just behind the jet shock we get

$$\nu'_{\rm b} = \frac{3q\sqrt{2\mu_{\rm o}u'_{\rm B}}}{4\pi m_{\rm e}}\gamma_{\rm max}^2, \tag{16}$$

where q is the elementary charge and $\mu_{\rm o}$ is the magnetic permeability of the vacuum. The steepening of the radio spectrum of the observed outbursts of microquasars strongly suggest that the observing frequency, ν, is close to the break frequency, i.e. $\nu \sim \nu'_{\rm b}\delta_\pm$. Therefore, if most of the observed emission comes from the region just behind the shock, we expect from Eq. (16) that $\gamma_{\rm max} \propto u'_{\rm B}(R_{\rm o})^{-1/4}$. This implies that $\gamma_{\rm max}$ and $u'_{\rm B}(R_{\rm o})$ are not independent parameters of the model but that they are correlated.

5. Application to GRS 1915+105

The number of parameters in the model outlined above is large. In order to reduce this number we assume that the jets in microquasars are freely expanding, i.e. $a_1 = 1$, and that the flux of magnetic energy through the jet is conserved, i.e. $a_2 = -2$. Since we assume the bulk velocity of the jet material to be constant, this implies that the ratio of the kinetic energy and the energy of the magnetic field is constant as well. Furthermore, we impose symmetry between the approaching and receding sides of the source in the sense that the model parameters describing the jet are the same on both sides. This may be a poor assumption as the jets of GRO J1655-40 are observed to be asymmetric (Hjellming & Rupen 1995). The model then depends on five free parameters: The e-folding distance of the number of relativistic particles within the jet accelerated by the shock, a_4, the bulk

velocity of the shocked jet material, $v_{\rm j}$, the maximum Lorentz factor up to which relativistic particles are initially accelerated, $\gamma_{\rm max}$, the slope of the initial power law energy spectrum of these particles, p, and the energy density of the magnetic field at $R_{\rm o}$, $u'_{\rm B}(R_{\rm o})$. The acceleration rate of relativistic particles at the normalisation radius, $\dot{N}'_{\rm o}(R_{\rm o})$, is in principle also a free parameter. However, from Eq.(15) we note that it is only a multiplicative factor in the calculation of the total radio emission of the jet. We therefore use it to normalise the model in such a way that for a given set of model parameters $\dot{N}'_{\rm o}(R_{\rm o})$ is such that the difference between the model predictions and the observational data is smallest for this given set of parameters.

Many radio outbursts of a number of microquasars have been observed. But to constrain the model parameters in a meaningful way, we would ideally need radio observations at two or more frequencies which clearly resolve the approaching and the receding jet component. Furthermore, the resolution should be sufficient to decide whether one of these jet components consists of multiple subcomponents, i.e. multiple shocks, the emission of which may be blended in observations of lower resolution. To date there are very few simultaneous multi-frequency observations which come even close to this ideal situation. The best studied radio outburst of any microquasar is still that of March 19th 1994 of GRS 1915+105 (Mirabel & Rodríguez 1994). This is also the outburst studied by Atoyan & Aharonian (1999). To test our model we will use the comparatively large data base accumulated during this event.

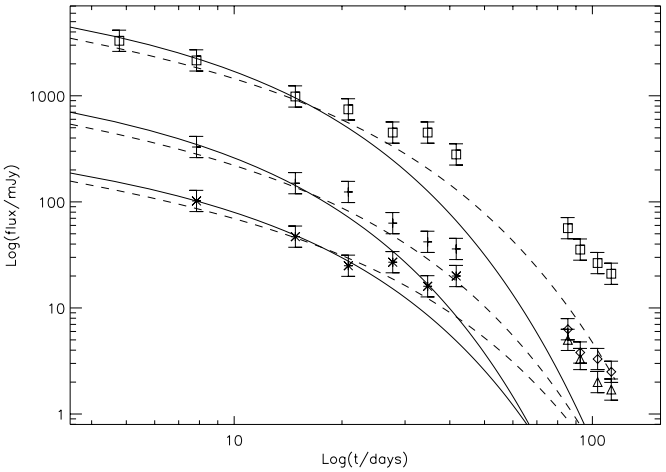

Fig. 1. Flux density measurements and model fits of the March 19 radio outburst of GRS 1915+105 at 8.4 GHz. Crosses and diamonds: Approaching jet component during first and second VLA campaign respectively, stars and triangles: receding jet component, same observations. Squares: Total radio flux at 8.4 GHz multiplied by a factor 5 for clarity. Solid lines: Predictions of the fiducial model fitted excluding flux measurements at 3.3 GHz for (from top to bottom) the total flux, the approaching and the receding jet component. Dashed lines: like solid lines but using all data for the model fit. Observations from Mirabel & Rodríguez (1994) and Rodríguez & Mirabel (1999).

5.1. The observations

The radio outburst of GRS 1915+105 which occurred in March 1994 was one of the strongest recorded for this object. The flux density at 1.4 GHz exceeded 1 Jy which is at least ten times higher than the radio flux in quiescence (Rodríguez et al. 1995). The outburst was observed with the VLA in A-array at 8.4 GHz during 7 epochs covering almost 42 days. Except for the first of these, the two jet components were resolved at this frequency (Mirabel & Rodríguez 1994). For the first unresolved and one further epoch measurements with the VLA are also available at 4.9 GHz and 15 GHz. In addition, GRS 1915+105 was monitored during this time by the Nancay telescope at 1.4 GHz and 3.3 GHz (Rodríguez et al. 1995). There are 24 flux measurements at each frequency but the source is unresolved at these frequencies. After a reconfiguration of the VLA four more observations of GRS 1915+105 of lower resolution were obtained at 8.4 GHz in B-array (Rodríguez & Mirabel 1999). These measurements cover roughly another 28 days but there is a gap of about 40 days between the end of the A-array observations and the start of the B-array campaign.

From the resolved VLA observations at 8.4 GHz Mirabel & Rodríguez (1994) determined a velocity for the jet components of 0.92 c and an angle of the jets to the line of sight of 70°. This assumes that the approaching and the receding component travel at the same velocity in opposite directions. Furthermore, it is assumed that GRS 1915+105 is located 12.5 kpc away from us. Fender et al. (1999) observed another radio outburst of GRS 1915+105 in October 1997 and found a higher intrinsic velocity which is inconsistent with a distance of 12.5 kpc. They argue that the most likely distance for this object is 11 kpc which then implies that the velocity of the jet components in March 1994 was 0.86 c and the angle of the jets to the line of sight is 68°. In the following we will adopt these later values. Extrapolating back the trajectories of the two jet components Mirabel & Rodríguez (1994) find that the outburst started at 20 hours on March 19.

Figs. 1 and 2 show all available flux density measurements as a function of time. Rodríguez & Mirabel (1999) note that another outburst of GRS 1915+105 occurred on April 21. The jet components of this new outburst are clearly visible as an unresolved emission peak coincident with the source centre in the VLA radio map of epoch 6. The approaching component of this new outburst is also distinctly visible on the map of the following observing epoch while the receding component is probably blended with that of the previous outburst of March 19. The signature of this later outburst as a sudden increase of the radio flux is not very distinct at 1.4 GHz and 3.3 GHz. Even at 8.4 GHz the situation in terms of the total flux density is somewhat unclear. However, the outburst can be easily identified as a separate event from the one of March 19 because the VLA maps reveal an emission peak distinct from those of the earlier outburst. The later observation epochs at the VLA with lower resolution detect the jet components of the April 21 burst while the components of the March 19 event were not detected (Rodríguez & Mirabel 1999). This is rather puzzling as the extrapolation of their lightcurves from the earlier observations indicate that they should still have been visible during these later observations.

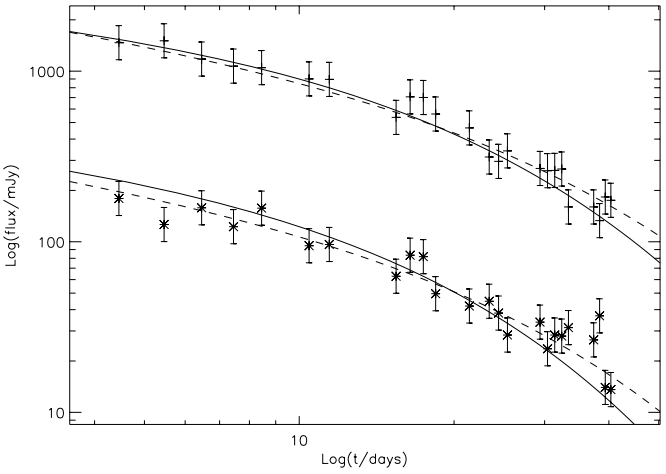

Fig. 2. Flux density measurements of the March 19 radio outburst of GRS 1915+105 at 1.4 GHz and 3.3 GHz. Crosses: Total radio flux at 1.4 GHz, stars: Total radio flux at 3.3 GHz divided by a factor 5 for clarity. Model predictions as in Fig. 1. Observational data from Rodríguez et al. (1995).

5.1.1. The blending of outbursts

A close examination of the total radio flux at 8.4 GHz reveals another sudden increase around observation epoch 4 (April 9, Fig. 1). This increase is also detected at 1.4 GHz and 3.3 GHz by the Nancay telescope on April 5 (Rodríguez et al. 1995, Fig. 2). Atoyan & Aharonian (1999) point out that this may be caused by a sudden additional injection of fresh relativistic electrons in the 'blobs' of gas they consider in their model. An alternative interpretation, which we will adopt here is that another, smaller outburst occurred shortly after April 4. In this case, the radio emission caused by the propagation of a new shock down the jet is most likely blended with that of the earlier event of March 19 because of the limited resolution of the observations. If the smaller outburst occurred at April 5, 0:0 hours, and assuming that the apparent shock velocity of this outburst is equal to that of the March 19 event, i.e. 17.5 mas day^{-1} (Rodríguez & Mirabel 1999), then the distance of the shock from the source centre on the approaching jet side at observing epoch 4 would be roughly 0.1". The position of the emission peak on April 9 is given as 0.36" from the source centre (Mirabel & Rodríguez 1994). The resolution of the VLA in A-array at 8.4 GHz is $\sim$0.3" and this means that a secondary peak caused by a later, somewhat weaker outburst as proposed here could not be detected as an individual structure. The situation on the receding jet side with its lower expansion velocities is even worse. However, the radio emission of the additional outburst would contribute to the total radio flux of the source and we believe that this has been detected here.

In summary, we will assume that the observations outlined above cover three separate radio outbursts of GRS 1915+105. The first and strongest occurred on March 19. The jet components of this burst are detected until the end of the first set of VLA observations (April 30). By the time of the second VLA campaign (June 13) they had vanished although the extrapolation of their earlier lightcurves suggested that they should still be observable. The second much weaker outburst occurred shortly after April 4, since the Nancay data show a sudden increase in radio flux on April 5 but not on April 4. The radio emission of this event is most likely blended with that of the first outburst and there is no sign of this second burst in the second set of VLA observations. The third outburst finally started on April 21 and was intermediate in strength. The radio emission caused by this event is clearly detected in the source centre on April 23 and the approaching jet component can be seen in the VLA map obtained on April 30. Both jet components are clearly detected in all four VLA observing epochs in June and July.

5.1.2. Data used in the modeling

In the continuous jet model for microquasars outlined above, only one shock is thought to travel outwards in each jet. Because of this, only observational data from observing epochs during which we can be sure that there was only one shock per jet contributing to the radio emission can be used in constraining the model parameters. From the above discussion it is clear that we can only use the three unresolved VLA measurements at 4.9 GHz, 8.4 GHz and 14.9 GHz from March 24 and the two following resolved observations at 8.4 GHz. These later observation provide us with separate flux measurements for the approaching and receding jet components. We also use the measurement of the receding jet component of April 9, since it seems likely that all the flux of the second outburst was attributed to the approaching component by Mirabel & Rodríguez (1994). Alternatively, this measurement can be taken as an upper limit. Of the Nancay observations we use all flux measurements starting March 24 through to April 4. There are eight observations during this time at 1.4 GHz and 3.3 GHz. For all 24 measurements used to constrain the model we assume the conservative error of 46% suggested by Rodriguez & Mirabel (1999) as opposed to the original error of 5% quoted by Rodríguez et al. (1995). In practice we did not use the eight 3.3 GHz data points as their inclusion led to significantly worse fits of the model to the observational data. See the next section for a discussion of this point.

5.2. Constraining the model parameters

We use the model outlined above to calculate the expected radio flux at the times GRS 1915+105 was observed during the outburst starting March 19. The 'goodness of fit' of the model for a given set of free parameters to the observations was assessed by calculating the sum of the χ^2-differences at the times the source was observed. The best-fitting model was then found by minimising this χ^2-value using a 4-dimensional downhill simplex method (Press et al. 1992). The remaining fifth model parameter, the energy density of the magnetic field at the normalisation radius, $u'_{\rm B}(R_{\rm o})$, was set 'by hand' to five different values. The normalisation radius, $R_{\rm o}$, was set to $1.1 \cdot 10^{14}$ m which corresponds to the unprojected distance of the jet shock from the source centre at the time of the first VLA observation, i.e. March 24.

Table 1. Results of the model fits. The first five fits are obtained without the 3.3 GHz data points. $u'_{\rm B}$ is the energy density of the magnetic field, a_4 is the radius beyond which the acceleration rate of relativistic particles decreases exponentially in units of $R_{\rm o}$ (see Eq. 6), $v_{\rm j}$ is the bulk velocity of the shocked jet material, $\gamma_{\rm max}$ is the initial high energy cut-off of the energy spectrum of the relativistic particles, p is the initial slope of this spectrum and $\dot{N}'_{\rm o}$ is its normalisation.

	$u'_{\rm B}(R_{\rm o})$/J m^{-3}	a_4	$v_{\rm j}$ / c	$\log(\gamma_{\rm max})$	p	χ^2	$\dot{N}'_{\rm o}(R_{\rm o})$
	$4.2 \cdot 10^{-7}$	2.8	0.61	3.2	1.4	0.26	$2.3 \cdot 10^{41}$
	$1.1 \cdot 10^{-5}$	2.7	0.61	2.9	1.4	0.26	$5.5 \cdot 10^{40}$
without 3.3 GHz data	$4.2 \cdot 10^{-5}$	$2.7^{+4.9}_{-1.0}$	$0.61^{+0.14}_{-0.13}$	$2.7^{+0.8}_{-0.36}$	$1.4^{+0.8}_{-0.9}$	0.26	$1.5 \cdot 10^{40}$
	$1.1 \cdot 10^{-3}$	2.7	0.61	2.4	1.4	0.26	$2.1 \cdot 10^{39}$
	$4.2 \cdot 10^{-3}$	2.6	0.61	2.2	1.4	0.26	$9.5 \cdot 10^{38}$
all data	$4.2 \cdot 10^{-5}$	4.2	0.56	2.8	1.9	1.02	$1.2 \cdot 10^{41}$

The results of the model fits are summarised in Table 1. The model fits the observational data equally well for all five adopted values for the strength of the magnetic field. As expected from Eq. (16) we find that the maximum Lorentz factor up to which relativistic particles are accelerated correlates strongly with the value of the energy density of the magnetic field. The values found for $\gamma_{\rm max}$ in the model fits follow almost exactly a $u'_{\rm B}(R_{\rm o})^{-0.25}$ law. This shows that the model presented here cannot be used to constrain the strength of the magnetic field within the jet independently of the maximum energy of the relativistic particles. To proceed we adopt in the following $u'_{\rm B}(R_{\rm o}) = 4.2 \cdot 10^{-5}$ as our fiducial model. This corresponds to the equipartition value of the magnetic field of 10^{-5} T (0.1 G) found by Atoyan & Aharonian (1999) for the chosen value of $R_{\rm o}$. Note however, that the energy density of the magnetic field and that of the relativistic particles does not stay in equipartition for all times in our model.

Figs. 1 and 2 show the model predictions of the fiducial model compared to the observational data. Also shown are the predictions of the model for the best-fitting parameters when using also the 3.3 GHz data. If we use all available data, the model predictions at the higher observing frequencies are rather low at early times. For the VLA measurements at 4.9 GHz and 14.9 GHz (not shown in Figs. 1 and 2) on March 24 the model predicts flux densities of 759 mJy and 385 mJy respectively. This is much lower than the measured flux densities of 887 mJy and 514 mJy at these frequencies. A closer inspection of Fig. 2 also shows that the measurement at 4.9 GHz actually exceeds those taken at 3.3 GHz at comparable times, which is unlikely to be real. Table 1 also shows that the fit obtained including the 3.3 GHz data is much worse in terms of the reduced χ^2-values than that excluding them. Also the flux densities predicted by our fiducial model which excludes the 3.3 GHz data, 926 mJy at 4.9 Ghz and 499 mJy at 14.9 Ghz, are much closer to the observations. Finally, the predictions of this model at 3.3 GHz fit the observations well at this frequency apart from the early observing epochs (see Fig. 2). We therefore believe that the model parameters found using our fiducial model and excluding the 3.3 GHz data are more reliable than those found when including these additional measurements.

To estimate the expected error of the model parameters of our fiducial model we calculated the χ^2-value for a large set of combinations of the 4 free model parameters. The uncertainties quoted in Table 1 are 1-σ errors corresponding to those parameter ranges for which $\chi^2 \leq 1$. Note that the uncertainties of the model parameters, particularly those of a_4 and p, are large while the light curves predicted by the model pass the data points well within the error bars of the flux measurements (see Figs. 1 and 2). This suggests that the quoted errors of the observed fluxes, at least for the VLA data points, are too conservative which also results in an overestimation of the uncertainties of the model parameters.

5.3. Comparison with the later observations

The exponential function which describes the change in the acceleration rate of relativistic particles as a function of the position of the shock in the jet, Eq. (6), implies that the radio flux caused by the first outburst on March 19 decreases quickly once $R_{\rm s}/R_{\rm o}$ exceeds a_4. This effect is clearly visible in Fig. 1 at 8.4 GHz. The model predicts that without the additional blended radio emission caused by the second and third outbursts around April 5 and April 21 the two jet components would have faded much more rapidly than is observed. This effect is less pronounced at lower frequencies (see Fig. 2). However, even for these the predicted and the observed light curves steepen somewhat roughly 15 days after the start of the first outburst. The continued steepening of the lightcurves of the two jet components at 8.4 GHz can also explain why they were not detected during the second observing campaign at the VLA (see Fig. 1).

We tried replacing the exponential in Eq. (6) with a simple power law. The data can be adequately fitted with this modified model as well. However, this change in the temporal behaviour of $\dot{N}'_{\rm o}(R_{\rm o})$ also leads to a much increased flux at low observing frequencies at later times. Using this modified model we found a flux at 1.4 GHz 40 days after the start of the first outburst exceeding the observations by a factor of at least 1.3 even without considering the possible contribution from later outbursts. This supports the picture of two colliding shells of jet material of finite width causing the internal shock. The rate at which energy is dissipated is roughly constant during the collision and decreases rapidly once the two shells have merged.

Comparing the model lightcurves with the observational data the signature of the second outburst starting around April 5,

about 16 days after the start of the first outburst, can clearly be detected at 8.4 GHz. The increase in the radio emission caused by the second event is less dramatic at 3.3 GHz and 1.4 GHz but can still be seen in Fig. 2. The third outburst of April 21, 32 days after the first burst, is seen as excess emission at 8.4 GHz and 3.3 GHz but is less obvious at 1.4 GHz. We note that in general the smooth lightcurve predicted by our model fits the VLA observations much better than the flux measurements at 1.4 GHz and 3.3 GHz taken with the Nancay telescope. This may imply larger errors for the low frequency data which hide to some extent the signatures of the second and third outburst which are much weaker than the first.

6. Properties of GRS 1915+105

6.1. Energetics

Using the model parameters of our fiducial model we now derive some of the physical properties of the jets of GRS 1915+105 during the outburst of March 19. The rate at which energy is transfered by the jet shock to the relativistic particle population at time $t'_{\rm s}$ is

$$\begin{aligned}\dot{E}'_{\rm rel} &= \dot{N}'_{\rm o}(R_{\rm o})e^{-R_{\rm s}/(R_{\rm o}a_4)}m_{\rm e}c^2\int_{\gamma_{\rm min}}^{\gamma_{\rm max}}\gamma_{\rm s}^{-p}(\gamma_{\rm s}-1)\,d\gamma_{\rm s}\\ &= 10^{29}e^{-R_{\rm s}/(R_{\rm o}a_4)}{\rm W},\end{aligned} \quad (17)$$

where we have assumed that only electrons and/or positrons are accelerated and that the initial energy spectrum of the relativistic particles extends down to $\gamma_{\rm min}=1$.

The rate at which energy is transported in the form of magnetic fields can be estimated by

$$\begin{aligned}\dot{E}'_{\rm B} &\approx \pi\left(\frac{\theta R_{\rm s}}{2}\right)^2 u'_{\rm B}(R_{\rm s})v'_{\rm s}\\ &= 1.8\cdot10^{28}\left(\frac{\theta}{\rm degrees}\right)^2{\rm W},\end{aligned} \quad (18)$$

where θ is the opening angle of the conical jet and $v'_{\rm s}$ is the speed of the shock in the frame of the shocked jet material. For our fiducial model $v'_{\rm s}=0.53$ c. Fender et al. (1999) find that during another outburst of GRS 1915+105 in 1997 θ was smaller than 8°. This would then imply an upper limit to $\dot{E}'_{\rm B}$ of $1.2\cdot10^{30}$ W. Note that the strength of the magnetic field in the jet after the passage of the shock is used here. This estimate does not imply that the unshocked jet material carries a magnetic field of this strength. Some or all of the magnetic field may be generated in the shock itself.

Finally, we can derive a lower limit for the bulk kinetic energy transported by the jet material. We know the number of relativistic light particles in the jet and so

$$\begin{aligned}\dot{E}_{\rm kin} &\geq (\gamma_{\rm j}-1)m_{\rm e}c^2\dot{N}'_{\rm o}(R_{\rm o})e^{-R_{\rm s}/(R_{\rm o}a_4)}\int_{\gamma_{\rm min}}^{\gamma_{\rm max}}\gamma_{\rm s}^{-p}\,d\gamma_{\rm s}\\ &= 6.3\cdot10^{26}e^{-R_{\rm s}/(R_{\rm o}a_4)}{\rm W}.\end{aligned} \quad (19)$$

This is only a strict lower limit, since we do not know whether the jets also contain thermal material and/or protons. In the case that there is one proton for each relativistic electron we find that the numerical constant in Eq. (19) increases to $1.2\cdot10^{30}$. Note that this then is identical to the energy carried in the form of magnetic fields for $\theta\sim8^\circ$.

The estimates for the energy transported along the jet in various forms presented above are lower by about a factor 10 than the estimates of Fender et al. (1999) for the weaker outburst in 1997. However, it should be noted that their estimates are based on the assumption that the radio emission is caused by two 'blobs' of relativistic plasma which were ejected by the central source within about 12 hours. The continuous jet model presented here requires that the estimated energy supply to the jet is sustained by the central source for at least 42 days; the length of the first observing campaign. This means that the total amount of energy produced by GRS 1915+105 is predicted by our model to be at least an order of magnitude greater during the March 1994 outburst than it was in the case of discrete ejections assumed for the September 1997 event.

These estimates illustrate that a continuous jet model cannot decrease the total amount of energy needed for a given radio outburst but the rate at which this energy is produced is much lower than in a model assuming discrete ejection events. This is the case because much, if not most, of the energy needed to produce the radio emission observed is 'stored' in the material of the continuous jet. This material was ejected by the central source during comparatively long period well before the process which led to the formation of the jet shock took place. Only the acceleration of relativistic particles at the jet shock then 'lights up' the jet and we are able to detect it.

6.2. Self-absorption

Since all jet properties are assumed to scale with distance from the source centre in our conical jet, it is clear that at some early time in the outburst the jet material was opaque for radio emission because of synchrotron self-absorption. The absorption coefficient in the rest frame of the emitting gas is given by (e.g. Longair 1981)

$$\begin{aligned}\chi'_{\nu'} &= 3.354\cdot10^{-9}\left(3.54\cdot10^{18}\right)^p\\ &\quad\times\kappa' B'^{(p+2)/2}b(p)\nu'^{(-p-4)/2}{\rm m}^{-1},\end{aligned} \quad (20)$$

where in our notation

$$\kappa' = \frac{4\dot{N}'_{\rm o}(R_{\rm o})\left(m_{\rm e}c^2\right)^{p-1}}{\pi v'_{\rm s}(R_{\rm s}\theta)^2}\,e^{-R_{\rm s}/(R_{\rm o}a_4)}, \quad (21)$$

and $b(p)$ is of order unity. We only consider the region just behind the jet shock where the energy distribution of the relativistic particles is completely described by a power law of exponent p. For a photon emitted at the centre of the jet the optical depth in the radial direction is then $\tau=R_{\rm s}\theta\chi'_{\nu'}/2$. For our fiducial model we then find that the jet material becomes transparent at 8.4 GHz roughly 2 hours after the start of the outburst when the shock has reached a distance of $\sim2\cdot10^{12}$ m from the source centre.

Mirabel et al. (1998) find that for the much weaker 'minibursts' of GRS 1915+105 the jets become transparent about 30

minutes after the start of the burst. Bearing in mind that the mini-bursts may be quite different in their properties compared to the major outburst considered here, our value is therefore in good agreement with their findings.

6.3. Infrared emission

Several groups have reported the detection of infrared emission from GRS 1915+105 (i.e. Sams et al. 1996, Mirabel et al. 1996, 1998). In the case of the mini-bursts simultaneous flux measurements at radio frequencies and in the K-band are available at times of about 10 to 20 minutes after the start of the bursts (Mirabel et al. 1996). Because of the uncertainties in the dust corrections in the K-band towards GRS 1915+105 it is difficult to estimate the spectral behaviour from radio to infrared wavelengths. However, for the mini-bursts flat spectra, $\alpha = 0$, regardless of the exact magnitude of extinction are observed very early during the bursts (Mirabel et al. 1996). The slope of the initial energy distribution of the relativistic particles in combination with the rather low high-energy cut-off of this distribution we found for our fiducial model is inconsistent with such flat emission spectra. However, this model does predict an unobscured, optically thin infrared flux of about 14 mJy in the K-band for a time about 15 minutes after the start of the burst. This may be enough to be detected in future observations of large outbursts. The timing requirements for such an observations are however difficult to meet, since the predicted infrared flux very quickly becomes undetectable at only slightly later times.

More puzzling is the detection of a resolved jet component with K-band flux of at least 1.8 mJy about 0.3" away from the centre of GRS 1915+105 by Sams et al. (1996). The shock on the approaching side of our jet model would need 24 days to reach such a large distance from the source centre. By this time our fiducial model predicts no synchrotron emission in the K-band at all. We have estimated whether this infrared emission may be caused by radio photons which are inverse Compton scattered to such high frequencies within the jet plasma. However, we find that this cannot explain the observations since the density of the relativistic particles in the jet in our model is orders of magnitude too low.

The observation of K-band emission far away from the core of GRS 1915+105 and the flat spectral indices of the mini-bursts suggest that two different types of outbursts may occur in the jets of this source. The strong radio bursts like the one of March 1994 are caused by jet shocks which produce large numbers of relativistic particles with a steep energy distribution. The weaker mini-bursts involve shocks which accelerate less particles but produce a flatter energy distribution which may also extend to higher energies than in the stronger bursts. The 'mini-burst mode' may correspond to a phase of relative stable jet production with only small variations in the bulk velocity of the jet material. Such flat spectra extending to millimeter wavelengths, possibly coupled with the continuous ejection of a jet, have been observed in Cygnus X-1 (Fender et al. 2000). The strong radio outbursts then probably mark phases of more violent changes in the central jet production mechanisms. Fender (1999) points out that this proposed behaviour may also be reflected in the X-ray signature of the accretion disk. In any case, other sources of infrared emission in the close vicinity of the jets like dust illuminated by the disk and/or the jet may further complicate the situation (Mirabel et al. 1996). To test the validity of the proposed scenario resolved observations of outbursts of GRS 1915+105 and other galactic jet sources from radio to infrared frequencies would be necessary.

7. The end of the jet

The energy transported by the jets of microquasars is enormous. This energy will be continuously deposited at the end of the jets and may lead to significant radiation from this region depending on how it is dissipated. In the following we investigate the fate of the energy transported by the jets of microquasars as predicted by our model. The discussion is based on the work by Leahy (1991).

7.1. Momentum balance

In order for the jets to expand they have to accelerate the surrounding ISM and push it aside. The velocity of the contact surface between the front end of the jet and the ISM, v_c, is given by balancing the momentum or 'thrust' of the jet material with the ram pressure of the receding ISM

$$\frac{v_\mathrm{c}}{v_\mathrm{j}} = \left(1 + \frac{1}{\Gamma_\mathrm{j} M_\mathrm{j}^2}\right) \times \left[1 + \sqrt{\frac{1}{\eta}\left(1 + \frac{1}{\Gamma_\mathrm{j} M_\mathrm{j}^2}\right)\left(1 + \frac{1}{\Gamma_\mathrm{c} M_\mathrm{c}^2}\right) - \frac{1}{\Gamma_\mathrm{j} M_\mathrm{j}^2}}\right]^{-1}, \tag{22}$$

where Γ_j and Γ_c are the adiabatic indices of the jet material and the ISM respectively, M_j is the internal Mach number of the jet flow, M_c is the Mach number of the contact surface with respect to the sound speed in the ISM and $\eta = \rho_\mathrm{j}/\rho_\mathrm{c}$. Here ρ_j is the mass density of the jet material while ρ_c is the density of the ISM. This expression is strictly valid only for non-relativistic jet velocities. However, since the bulk velocity of the shocked jet material, v_j, is only mildly relativistic in our fiducial model, $\gamma_\mathrm{j} = 1.3$, we take Eq. (22) to be a good approximation. Note that the velocity of the jet material in front of the shock is even lower than v_j.

For $v_\mathrm{c} \sim v_\mathrm{j}$ the jet material does not decelerate strongly at the end of the jet. This implies that little of the kinetic energy transported by the jet is dissipated. Even for large internal Mach numbers it is then unlikely that a strong shock will develop in the jet flow close to the contact surface. This occurs when the jet is overdense, i.e. $\eta \gg 1$ and so the jet flow is close to being ballistic. For underdense jets, $\eta < 1$, the ratio $v_\mathrm{c}/v_\mathrm{j}$ can become considerably smaller than 1. In this case a strong deceleration of the jet ensues and much of its kinetic energy is dissipated. For $M_\mathrm{j} \gg 1$ a strong shock will form and can act as a site of efficient acceleration of relativistic particles. Examples for this are the

powerful extragalactic radio sources of type FRII (Fanaroff & Riley 1974) with their very bright radio hot spots at the end of their jets. The diffuse radio lobes enveloping their jets are the remains of the shocked jet material left behind by the advancing contact surface. In the transonic regime, $M_\mathrm{j} \sim 1$, only weak shocks may form at the jet end and particle acceleration is less efficient. The less powerful jets of FRI objects fall in this class.

7.2. Application to our fiducial model

In the model developed in the previous sections we have assumed the jets of microquasars to be conical with a constant opening angle. This implies $\eta = \eta_\mathrm{o}(R/R_\mathrm{o})^{-2}$ and, because of the adiabatic expansion of the jet material, $M_\mathrm{j} = M_\mathrm{j}(R_\mathrm{o})(R/R_\mathrm{o})^{\Gamma_\mathrm{j}-1}$. The bulk velocity of the jet material is high in our fiducial model and unless the jet material is very hot ($T_\mathrm{j}(R_\mathrm{o}) > 10^{12}$ K in the case of a proton-electron jet) the internal Mach number of the jet flow will always greatly exceed 1. Since η is a strongly decreasing function of R, we expect from Eq. (22) that the ratio $v_\mathrm{c}/v_\mathrm{j}$ will always fall significantly below unity for large values of R. This means that the jets of microquasars should end eventually in strong shocks which may be detectable in the radio. In the source XTE J1748-288 a region of bright radio emission was observed to slow down and brighten at the same time some distance from the centre of the source (Hjellming et al. 1999). In our model this is interpreted as an internal shock reaching the end of the jet where the termination shock further boosts the relativistic particle population which was pre-accelerated by the internal shock. After passing through the termination shock the jet material may inflate a radio lobe very similar to extragalactic FRII objects if $v_\mathrm{c}/v_\mathrm{j} \ll 1$ (see also Levinson & Blandford 1996a, b). It has been suggested that the diffuse radio emission region W50 around SS433 is the radio lobe inflated by the jets of this source (Begelman et al. 1980). Other radio lobes were detected around 1E 1740.7-2942 (Mirabel et al. 1992), GRS 1758-258 (Rodríguez et al. 1992) and possibly GRO J1655-40 (Hunstead et al. 1997), but not in the vicinity of GRS 1915+105 (Rodríguez & Mirabel 1998). The absence of a radio lobe in GRS 1915+105 may indicate that the jet in this source is relatively young and has not yet reached the point at which it becomes underdense with respect to the ISM. In the following we estimate the distance out to which the jets in this source may travel without the formation of a strong termination shock.

A lower limit for η can be derived from our fiducial model assuming that the jets consist only of the relativistic particles responsible for the synchrotron emission plus the particles needed for charge neutrality. Thus

$$\eta \geq \dot{N}'_\mathrm{o}(R_\mathrm{o}) e^{-R_\mathrm{s}/(R_\mathrm{o} a_4)} \frac{m_\mathrm{j}}{\pi \left(\theta/2R_\mathrm{s}\right)^2 v'_\mathrm{s} \rho_\mathrm{c}} \int_{\gamma_\mathrm{min}}^{\gamma_\mathrm{max}} \gamma_\mathrm{s}^{-p}\, d\gamma_\mathrm{s}, \tag{23}$$

where m_j is the mass of the average particle in the jet. An upper limit for η can be derived from the assumption that the rate at which mass is ejected along the jet can not exceed the mass accretion rate within the disk powering the jet. Fits to the X-ray spectrum of GRS 1915+105 suggest an accretion rate of order $\dot{m} \sim 10^{15}$ kg s^{-1} (Belloni et al. 1997). We then find

$$\eta \leq \frac{\dot{m}}{\pi \left(\theta/2R_\mathrm{s}\right)^2 v'_\mathrm{s} \rho_\mathrm{c}}. \tag{24}$$

Note that this upper limit does not depend on the nature of the jet material. Using Eqs. (23) and (24) and assuming $\rho_\mathrm{c} \sim m_\mathrm{p} 10^6$ kg m^{-3}, corresponding to a particle density of 1 cm^{-3}, we find $56 \leq \eta_\mathrm{o} \leq 1300$ for a proton-electron jet and $0.03 \leq \eta_\mathrm{o} \leq 1300$ for a pair plasma jet. The lower limit for the pair plasma jet assumes that the pairs are cold. Because of pair annihilation it is unlikely that the material of a pair plasma jet is cold (e.g. Gliozzi et al. 1999) and so this lower limit is used here for illustrative purposes only. Relativistic thermal motion of the pairs would raise this lower limit.

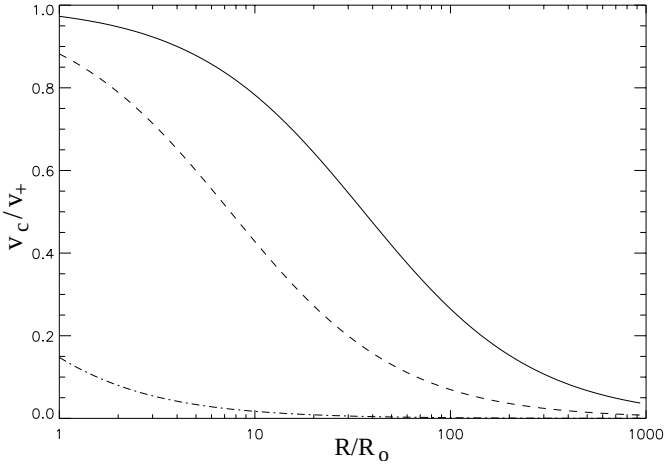

Fig. 3. The advance speed of the termination shock at the end of a hypersonic, conical jet in units of the bulk velocity of the jet material. Solid line: The case of maximum mass transport rate. Dashed line: Minimum mass transport rate of a proton-electron jet. Dot-dashed line: Minimum mass transport rate for a pair plasma jet.

For the reasonable assumptions $M_\mathrm{c} \gg 1$ and $M_\mathrm{j} \gg 1$ Fig. 3 shows the ratio $v_\mathrm{c}/v_\mathrm{j}$ as calculated from Eq. (22). We see that even if the mass transport rate of the jet is equal to the mass accretion rate a termination shock should form about $50R_\mathrm{o} \sim 5 \cdot 10^{15}$ m away from the core of the source. This distance is reached by the jet material traveling at $v_\mathrm{j} = 0.61$ c in less than two years.

GRS 1915+105 was discovered as a bright X-ray source on the 15th of August 1992 (Castro-Tirado et al. 1992). Given the availability of X-ray monitoring satellites before 1992 it is not likely that this source was very active before this date. The subsequent radio monitoring with the Green Bank Interferometer (e.g. Foster et al. 1996) shows that after its discovery GRS 1915+105 produced radio outbursts every few months. In the frame of the internal shock model described here this implies that jet production must have been reasonably steady since 1992. Assuming that the bulk velocity of the jet material did not vary strongly, the end of the jet must have reached a distance of roughly $3 \cdot 10^{16}$ m from the core by the end of 1997. This is

the time of the radio observation of the large scale surroundings of GRS 1915+105 by Rodríguez & Mirabel (1998) who did not find any evidence for a termination shock of the jet or radio lobes (but see Levinson & Blandford 1996a).

The estimation of the position of the termination shock depends crucially on the overdensity of the jet material with respect to the ISM. It is possible that the gas density in the vicinity of GRS 1915+105 is lower than assumed here. However, given its location in the galactic plane this is rather unlikely. A further possibility is that the jets of microquasars are not conical for their entire length. The jets of extragalactic FRII objects are believed to pass through a very oblique reconfinement shock which brings them into pressure equilibrium with their environment (e.g. Falle 1991). These shocks are not very efficient in accelerating relativistic particles and so are often undetectable. This scenario is also confirmed for FRII sources by numerical simulations of their jets (e.g. Komissarov & Falle 1998). The same process may recollimate the jets of microquasars as well. In this case they may stay overdense with respect to the ISM much longer and this would enable them to travel out to much larger distances before terminating in a strong shock. In this respect it is interesting to note that Rodríguez & Mirabel (1998) found a compact non-thermal emission region located 16.3' away from GRS 1915+105. The feature is elongated and its major axis is aligned with one of the jets. If this feature is caused by the jet pointing in its direction then it must have been ejected by the core roughly 280 years ago. This may be the time scale on which GRS 1915+105 becomes active and produces jets.

8. Observational tests of the model

8.1. Emission lines

In our model the jet flow initially consists of non-relativistic hot plasma. Due to adiabatic expansion losses of thermal energy during the propagation of this material along the conical jet with given opening angle, the temperature of the plasma decreases. Internal shocks as envisioned above lead to local heating and acceleration of relativistic particles but do not change this general picture. In reality the situation is very similar to that in the well-known source SS433. In SS433 we observe bright optical recombination Balmer, Paschen and Brackett lines of hydrogen which are blue-shifted in the approaching jet and red-shifted in the receding jet. The velocity of the jet flow in SS433 is equal to 0.26 c. Due to the precession of the jet the observed red and blue shifts are strong functions of time (Margon 1984). In our case the inclination angle of the jets of GRS 1915+105 is known from the observations by Mirabel & Rodríguez (1994). This angle, $\theta = 68^\circ$, and the bulk velocity of 0.6 c of the jet material found in our fiducial model permits us to estimate the red and blue line shifts of the emitting jet material:

$$\frac{\lambda}{\lambda'} = \gamma_j(1 \pm \beta_j \cos\theta) \; = \; \begin{cases} 0.97 \; ; \text{approaching} \\ 1.53 \; ; \text{receding} \end{cases} \qquad (25)$$

Note that any line emission coming from the jet approaching the observer is hardly shifted in wavelength at all. Assuming that the bulk velocity of the jet material in the jets of GRO J1655-40 is also close to 0.6 c, we find for this source that the emission lines are redshifted for the approaching jet ($\lambda/\lambda' \sim 1.18$) as well as for the receding jet ($\lambda/\lambda' \sim 1.32$). This is caused by the large viewing angle, $\theta = 85^\circ$, of the jets in this object (Hjellming & Rupen 1995). In both cases the very large inclination angles result in a strong predicted asymmetry in the line shifts for the two jets. Measuring these shifts will permit us to estimate both the velocity of the jet bulk flow and the viewing angle θ. Furthermore, any jet precession as in the case of SS433 could be detected.

Measuring the predicted line shifts is complicated by the low density of the material in the jet flow of SS433 and GRS 1915+105 which prevents the production of bright recombination lines. However, we know that in the case of SS433 there is a strong thermal instability in the flow which leads to the formation of small, dense cloudlets (Panferov & Fabrika 1997). This increases the recombination rate and effective emission measure of the plasma in the flow. If there is a similar instability in the jets of GRS 1915+105 and GRO J1655-40 we have a good chance to observe recombination lines from both of these sources. Another problem is the strong obscuration of GRS 1915+105 by interstellar dust. Therefore, it is only possible to look for recombination lines of hydrogen in the K-band. In the case of GRO J1655-40 obscuration is low and there is a chance to detect Lyman and Balmer lines. Unfortunately, the mechanical power of the jet in GRO J1655-40 is smaller than in GRS 1915+105 or SS433. This will lead to a smaller density and emission measure of the jet material and therefore also a smaller intensity of the lines. It is important to bear in mind that in SS433 the emission lines are extraordinarily bright but modern observational techniques permit us to look for blue and red-shifted lines which are weaker by many orders of magnitude.

In SS433 ASCA discovered red and blue-shifted X-ray K-lines of iron with a rest energy of roughly 6.7 keV and similar lines of hydrogen- and helium-like sulphur and argon (Kotani et al. 1997). In our case the cooling jet flow with an initially very high temperature must lead to the emission in similar lines of recombining high-Z ions. Again, the mechanical energy of the flows in GRS 1915+105 and GRO J1655-40 is smaller than in SS433 and, therefore, the lines should be weaker in these objects. However, the new X-ray spacecraft, XMM, CHANDRA, ASTRO-E, Constellation-X and XEUS, may be able to detect such emission in red and blue-shifted X-ray lines. Note in this respect the detection of shifted iron lines in GRO J1655-40 reported by Bałucińska-Church & Church (2000) with RXTE which the authors attribute to the accretion disk but may very well originate in the continuous jets of this source.

All predictions for the production of line emission in the jets are based on the assumption that the jet flow consists of matter with a high but non-relativistic temperature moving as a whole with relativistic bulk velocities. There are two other obvious possibilities: (i) The jet matter consists of a pair plasma and (ii) the jets consist only of ultra-relativistic plasma with no cold electrons present. In case (i) we have to consider the possibility of a bubble around an X-ray source filled with a huge amount

of positrons. If these positrons become non-relativistic due to adiabatic or other energy losses inside the jets and they cool down to sufficiently low temperatures, we may observe a blue and red-shifted recombination line of positronium in the optical and UV wavebands. This line has a wavelength twice that of the Ly-α line of hydrogen. Much more important in this case, annihilation lines could be observed again red and blue-shifted relative to the rest energy of 511 keV. The strong red-shift but weak blue-shift of this line predicted by our model leaves a unique signature which will be observable with INTEGRAL. A luminosity only a few times smaller than the mechanical power of the jets will be emitted in the electron-positron annihilation line in this case. This large luminosity should make the annihilation lines observable despite the unfavorable angle of the jets to our line of sight. In the case of only ultra-relativistic plasma in the jets, case (ii), no recombination or annihilation lines should be observable.

8.2. Radio continuum

The internal shock models of GRBs (Rees & Meszaros 1994) attribute the formation of the shock traveling along the jet to the collision of shells of jet material with different bulk velocities. In the non-relativistic limit the velocity of the resulting shock is governed by the same momentum balance, Eq. (22), as the velocity of the termination surface of the jet. All quantities in that equation with subscript 'c' now refer to the slower jet material in front of the jet shock while those with subscript 'j' denote properties of the faster jet material driving the shock. The density ratio η is now simply given by the densities of the faster jet material driving the shock, ρ_2, and that of the slower gas in front of the shock, ρ_1. We already pointed out in Sect. 7.1 that the jet shock is likely to be strong and so both Mach numbers in Eq. 22 are significantly greater than unity. Therefore $v_{\rm s} \sim v_{\rm j}\left(1+1/\sqrt{\eta}\right)^{-1}$. Since in our model all material is assumed to be part of the conical jet structure, we find $\rho_1 \propto \rho_2 \propto R^{-2}$ and therefore $\eta = \rho_1/\rho_2 = {\rm const.}$. This implies that within the limitations of the model presented here the velocity of the shock is constant as well which is confirmed by the observations (e.g. Mirabel & Rodríguez 1999 and references therein).

Once the energy of the shell collision is spent, the shock emission fades rapidly. It is therefore possible that we can observe the shock reaching the end of the jet only in special cases (XTE J1748-288, Hjellming et al. 1999; see above). We would then expect that the superluminal component should brighten, as well as decelerate rather abruptly. In the plasmon model the observed constant superluminal motion is taken to indicate a large mass and consequently large kinetic energy of the plasmon. If a plasmon is observed to slow down because of the growing mass of ISM it sweeps up, then this deceleration should be rather gradual unless the plasmon encounters a local overdensity in the ISM. The observed deceleration of the superluminal component in XTE J1748-288 occurred rather rapidly at a distance of about 1" from the core after a phase of expansion with practically constant velocity. Furthermore, the emission region is still detected in recent observations; 15 months after the start of the burst (Rupen, private communication). During this time it appears to have advanced only slowly at a velocity of about 0.01" per month or roughly 5000 km s^{-1}. This slow motion and persistent radio emission may be interpreted as arising from the shock at the end of a continuous jet (see the previous section).

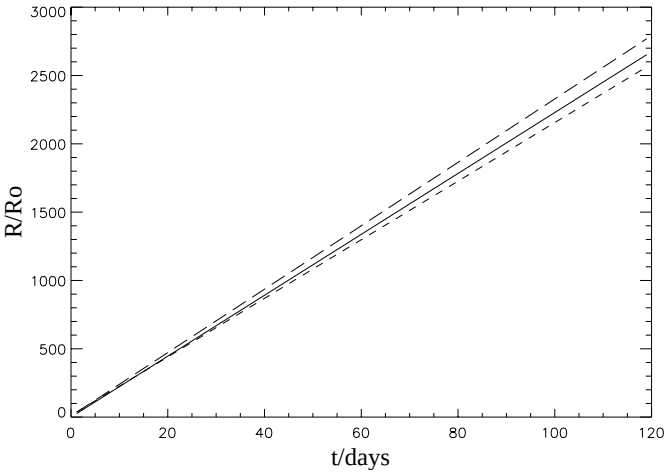

Fig. 4. Position of the radio emission peak in the fiducial model as a function of time after the start of the outburst. Solid line: Velocity of the jet shock derived from the 8.4 GHz observations, dashed line: Model prediction at 1.4 GHz and long dashed line: Model prediction at 8.4 GHz. Only the approaching jet component is plotted.

Some interesting predictions can be made from the model for future radio observations in the case that these can resolve the approaching and receding jet components along the jet axis. Because of the way in which the rate of acceleration of relativistic particles in the jet by the shock varies with time, the peak of the radio emission is not coincident with the position of the shock. This off-set depends on the observing frequency in the sense that the lower this frequency the more the emission peak lags behind the leading shock. This is illustrated in Fig. 4 where we plot the distance of the emission peak on the approaching jet side as a function of time for two different frequencies. Note also that this effect predicts that we should measure slightly different advance velocities of the emission peaks at different frequencies. This will not be observed in the case of discrete plasmon ejections.

The steepening of the radio spectrum of the jets in microquasars in this model is explained by the superposition of the contribution to the total emission from various regions within the jet. In resolved radio maps of the jet components this should be visible because the model predicts the radio spectral index to change along the jet axis. This behaviour is shown in Fig. 5 for the approaching jet. Fig. 5 also shows the distribution of the flux along the jet axis. The relatively uniform distribution is caused by the decrease of the magnetic field strength further out along the jet counteracting the injection of newly accelerated particles by the shock. The jet region over which the spectrum steepens is small and the emission originating in this region also weakens considerably in the direction away from the jet shock. This may make a detection of the spectral steepening along the jet diffi-

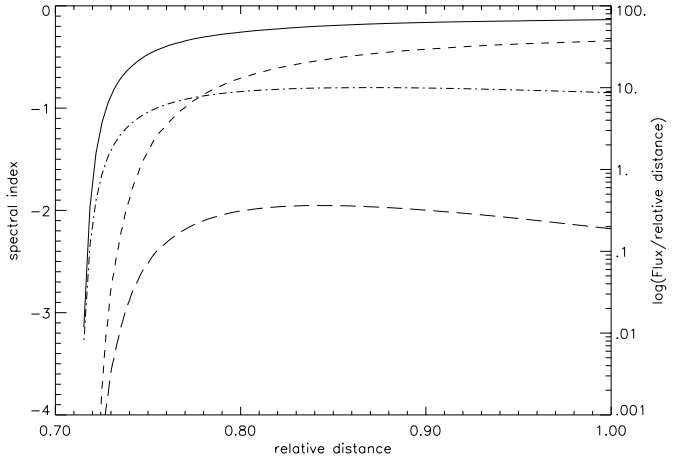

Fig. 5. Predicted variation of the radio spectral index between 1.4 GHz and 8.4 GHz and flux along the jet axis. The length scale on the x-axis is normalised to the distance of the jet shock from the source centre at the respective observing time. Solid line: At the time of the first VLA observations, i.e. 4.8 days after the start of the outburst. Short-dashed line: At a time of 40 days after the start of the outburst. Dot-dashed line: Flux per relative distance in arbitrary units at 8.4 GHz at the time of the first VLA observations, corresponding to solid line. Long-dashed line: Flux per relative distance 40 days after the start of the outburst, corresponding to short-dashed line.

cult. However, the apparent shortening of the emission region along the jet at higher observing frequencies may be detectable. The decrease in the strength of the magnetic field combined with the high energy cut-off of the energy spectrum of the relativistic particles leads to an overall steepening with time of the radio spectrum along the jet axis. This is also shown in Fig. 5 and should be observable if the jet components can be resolved at more than one frequency.

Note also that the length of the region along the jet axis which is emitting radiation at a given frequency increases with time. Although the fraction of the distance of the shock from the source centre subtended by the emitting region shrinks for later times (see Fig. 5), the absolute extent of this region will grow. This may also be detectable in future radio observations of sufficient surface brightness sensitivity.

Another prediction of the model is that the lightcurves of radio outbursts in microquasars at a given observing frequency should have a fairly constant slope for a few tens of days. After that they steepen rapidly once the critical frequency of the most energetic relativistic particles moves below the observing frequency. This steepening occurs earlier at higher frequencies. At the same time that the steepening of the lightcurves occurs, the flux ratio of the approaching and receding jet components should decrease. This effect is seen in Fig. 1. The jet components of the second outburst of April 21 observed during the second observing campaign with the VLA (Rodríguez & Mirabel 1999) show a much steeper lightcurve than those of the first outburst and, at the same time, a smaller flux ratio. Since these components were observed later in their evolution than those of the first outburst, this is in agreement with the predictions of the model.

9. Conclusions

We developed a continuous jet model for the radio outbursts of galactic microquasars. The model naturally explains the observed rather flat decaying lightcurves of these bursts as the signature of synchrotron radiation of relativistic particles accelerated by internal shocks in the conical jets. The comparatively long duration of the bursts implies that this model is a 'time-resolved' version of the internal shock model proposed for GRB (Rees & Meszaros 1994), though the synchrotron emission is produced at much lower frequencies. The gradual steepening of the radio spectrum is explained by a superposition of the radiation of different populations of relativistic particles with different ages. This spectrum of ages results from the shock traveling along the jet with older populations of accelerated particles left behind.

We find that only a roughly constant rate of acceleration of relativistic particles followed by an exponential decay can explain the observed light curves for the strong outburst of GRS 1915+105 in 1994. We interpret this behaviour as the signature of two colliding shells of jet material, as in the internal shock model for GRB. A consequence of this is the continued steepening of the lightcurves of a given outburst coupled with a decreasing flux ratio of the emission observed from the approaching to that from the receding jet side.

The energy requirements of the continuous jet model for producing radio outbursts are similar to those of the plasmon model. However, much of the energy underlying the outbursts may be stored in the continuous jet while the passage of the internal shock only 'lights up' the jet. This implies that the rate at which the energy of the outburst is supplied by the central engine to the jet is much lower than in the plasmon model.

The occurrence of mini-bursts in microquasars with flat spectra up to infrared frequencies (Mirabel et al. 1998) and the observation of K-band emission in the jet a considerable distance away from the core (Sams et al. 1996) suggest different modes of jet production: (i) A stable 'mini-burst' mode with relative little variation in the bulk jet speed and therefore also only weak internal shocks. (ii) A more variable outburst mode with strong variations in the jet speed and strong internal shocks (see also Fender 1999). The weaker flavour internal shocks seem to produce flatter relativistic particle spectra extending to higher energy compared to the strong shocks. However, the total number of accelerated particles must be much larger in the strongly variable phase.

We show that the properties of the continuous jets of microquasars should lead to strong shocks at their ends where they are in contact with the surrounding ISM. This is consistent with the recent observations of the decelerating radio emission region of XTE J1748-288 (Hjellming et al. 1999) and its persistence for 15 months after the start of the original outburst (Rupen, private communication). The shocked jet material may subsequently inflate a low density cavity around the jets similar to the radio lobes in extragalactic jet sources of type FRII. This is observed in SS433 (Dubner et al. 1998) and may be in a few other microquasars. The absence of such shocks and radio

lobes in GRS 1915+105 may indicate that the jets in this source are young and/or that they recollimate because of the pressure of their environment. If this is the case then the detection of a non-thermal emission region in the more extended environment of GRS 1915+105 (Rodríguez & Mirabel 1998) may imply a recurrence time of the jet activity scale of ~ 280 years.

Many of the predictions of this model for microquasars can be tested observationally. However, to clearly distinguish between this model of continuous jets and the plasmon model it would be necessary to spatially resolve the superluminal emission regions during outbursts, preferentially at more than one radio frequency. Additional support for the scenario of continuous jets may come from further high resolution observations of the cores of microquasars during quiescence. These should show at least some spatial extension of the radio emission along the jet axis as observed in Cygnus X-1 (Fender et al. 2000). These observations can potentially provide us with valuable information on the properties of the jets which otherwise we can only study during strong outbursts when strong shocks pass through them.

Acknowledgements. The authors would like to thank G. Ghisellini and the referee, L.F. Rodríguez, for valuable discussions which improved the paper. This work was partly supported by EC grant ERB-CHRX-CT93-0329 within the research network 'Accretion onto compact objects and proto-stars'

References

Atoyan A.M., Aharonian F.A., 1999, MNRAS 302, 253
Bałucińska-Church M., Church M.J., 2000, MNRAS accepted, astro-ph/9912389
Begelman M.C., Sarazin C.L., Hatchett S.P., McKee C.F., Arons J., 1980, ApJ 238, 722
Belloni T., Mendez M., King A.R., van der Klis M., Paradijs J.V., 1997, ApJ 488, L109
Blandford R.D., Rees M.J., 1974, MNRAS 169, 395
Castro-Tirado A., Brandt S., Lund N., 1992, IAU Circ. 5590
Drury L.O'C., 1983, Rep. Prog. Phys. 46, 973
Dubner G.M., Holdaway M., Goss W.M., Mirabel I.F., 1998, AJ 116, 1842
Falle S.A.E.G., 1991, MNRAS 250, 581
Fanaroff B.L., Riley J.M., 1974, MNRAS 167, 31
Fender R.P., 1999, In: Kaper L., van den Heuvel E.P.J., Woudt P.A. (eds.) Black holes in binaries and galactic nuclei. Springer in press
Fender R.P., Garrington S.T., McKay D.J., et al., 1999, MNRAS 304, 865
Fender R.P., Pooley G.G., Durouchoux P., Tilanus R.P.J., Brocksopp C., 2000, MNRAS 312, 853
Foster R.S., Waltman E.B., Tavani M., et al., 1996, ApJ 467, L81
Ghisellini G., 1999, Astron. Nachr., submitted, astro-ph/9906145
Ghisellini G., Maraschi L., Treves A., 1985, A&A 146, 204
Gliozzi M., Bodo G., Ghisellini G., 1999, MNRAS 303, L37
Heavens A.F., Meisenheimer K., 1987, MNRAS 225, 335
Hjellming R.M., Johnston K.J., 1988, ApJ 328, 600
Hjellming R.M., Rupen M.P., 1995, Nat 375, 464
Hjellming R.M., Rupen M.P., Mioduszewski A.J., et al., 1999, American Astronomical Society Meeting 193, 103.08
Hunstead R.W., Wu K., Campbell-Wilson D., 1997, In: Wickramasinghe D.T., Ferrario L., Bicknell G.V. (eds.) Accretion phenomena and related outflows. ASP Conference Series, p. 63
Kaiser C.R., Dennett-Thorpe J., Alexander P., 1997, MNRAS 292, 723
Komissarov S.S., Falle S.A.E.G., 1998, MNRAS 297, 1087
Kotani T., Kawai N., Matsuoka M., Brinkmann W., 1997, In: Wickramasinghe D.T., Ferrario L., Bicknell G.V. (eds.) Accretion phenomena and related outflows. ASP Conference Series, p. 270
Leahy J.P., 1991, In: Hughes P.A. (ed.) Beams and jets in astrophysics. Cambridge University Press, p. 100
Levinson A., Blandford R., 1996a, A&AS 120, 129
Levinson A., Blandford R., 1996b, ApJ 456, L29
Longair M.S., 1981, High energy astrophysics. Cambridge University Press
Margon B., 1984, ARA&A 22, 507
Marscher A.P., Gear W.K., 1985, ApJ 298, 114
Mirabel I.F., Rodríguez L.F., 1994, Nat 371, 46
Mirabel I.F., Rodríguez L.F., 1998, Nat 392, 673
Mirabel I.F., Rodríguez L.F., 1999, ARA&A 37, 409
Mirabel I.F., Rodríguez L.F., Cordier B., Paul J., Lebrun F., 1992, Nat 358, 215
Mirabel I.F., Rodríguez L.F., Chaty S., et al., 1996, ApJ 472, L111
Mirabel I.F., Dhawan V., Chaty S., et al., 1998, A&A 330, L9
Panferov A.A., Fabrika S.N., 1997, Astronomy Reports 41, 506
Press W.H., Teukolsky S.A., Vetterling W.T., Flannery B.P., 1992, Numerical Recipes. Second edition, Cambridge University Press, Cambridge, UK
Rees M.J., 1978, MNRAS 184, P61
Rees M.J., Meszaros P., 1994, ApJ 430, L93
Reynolds C.S., Begelman M.C., 1997, ApJ 487, L135
Rodríguez L.F., Mirabel I.F., 1998, A&A 340, L47
Rodríguez L.F., Mirabel I.F., 1999, ApJ 511, 398
Rodríguez L.F., Mirabel I.F., Martí J., 1992, ApJ 401, L15
Rodríguez L.F., Gerard E., Mirabel I.F., Gómez Y., Velázquez A., 1995, ApJ 101, 173
Rybicki G.B., Lightman A., 1979, Radiative Processes in Astrophysics. Wiley, New York
Sams B.J., Eckart A., Sunyaev R., 1996, Nat 382, 47
Shu F.H., 1991, The physics of astrophysics. Vol.1, Radiation. University Science Books, Mill Valley
van Paradijs J., 1995, In: Lewin W.H.G., van Paradijs J., van den Heuvel E.P.J. (eds.) X-ray binaries. Cambridge University Press, p. 536